JOURNAL OF GEOPHYSICAL RESEARCH, VOL. 108, NO. D19, 4610, doi:10.1029/2002JD002986, 2003

Stratospheric drain over Indonesia and dehydration within the tropical tropopause layer diagnosed by air parcel trajectories

Hiroaki Hatsushika
Central Research Institute of Electric Power Industry, Abiko Research Laboratory, Abiko, Japan

Koji Yamazaki
Graduate School of Environmental Earth Science, Hokkaido University, Sapporo, Japan

Received 27 September 2002; revised 27 June 2003; accepted 16 July 2003; published 10 October 2003.

[1] The structures of temperature and velocity fields in the tropical tropopause layer (TTL) in boreal winter are investigated using an atmospheric general circulation model (AGCM). The model reveals strong upward motions in the lower part of the TTL over the maritime continent and the western tropical Pacific, corresponding to the ''stratospheric fountain'' region, and downward motions in the upper part of the TTL over Indonesia, representing the stratospheric drain. In the TTL, strong easterlies prevail, and the cold ascent region tilts eastward. A down-slope flow over the upward-bulging isentropic surface produces the downward p velocity over Indonesia. In addition, reduction of longwave heating over deep convection suppresses the upward motion. The model simulates the observed stratospheric drain signature well, without convective overshootings. A trajectory analysis using the AGCM-simulated three-dimensional wind and temperature is performed to clarify the entry process of air parcels from the tropical troposphere to the stratosphere and to investigate the dehydration process during passage through the TTL. Tropospheric air parcels are advected upward to the bottom of the TTL mainly from the stratospheric fountain region. A pair of anticyclonic circulations in the tropical western Pacific entrains air parcels, which then pass through the equatorial cold region several times during the slow ascent in the TTL. This slow spirally ascending motion brings about low humidity in the stratosphere, despite the local downward motion over Indonesia. In addition, transient disturbances, particularly low-frequency disturbances, produce intermittent upward motions over the fountain region, resulting in effective dehydration of the air. The spiral ascent and transient mechanisms are key factors in the dehydration process in the TTL. The interannual variation in the water vapor mixing ratio into the tropical lower stratosphere with the El Niño/Southern Oscillation cycle is also estimated, and it is found that in La Niña years, air is more dehydrated. *INDEX TERMS:* 0341 Atmospheric Composition and Structure: Middle atmosphere—constituent transport and chemistry (3334); 3334 Meteorology and Atmospheric Dynamics: Middle atmosphere dynamics (0341, 0342); 3362 Meteorology and Atmospheric Dynamics: Stratosphere/troposphere interactions; *KEYWORDS:* stratospheric fountain, tropical tropopause layer, trajectory analysis

Citation: Hatsushika, H., and K. Yamazaki, Stratospheric drain over Indonesia and dehydration within the tropical tropopause layer diagnosed by air parcel trajectories, *J. Geophys. Res.*, *108*(D19), 4610, doi:10.1029/2002JD002986, 2003.

1. Introduction

[2] The ''stratospheric fountain'' hypothesis, which asserts that the entry of water vapor from the troposphere into the stratosphere is limited to the western tropical Pacific, northern Australia, Indonesia, and Malaysia in boreal winter, was proposed by *Newell and Gould-Stewart* [1981] to account for the low observed stratospheric humidity. This concept has enjoyed general acceptance until quite recently. The fountain hypothesis, based on an analysis of global 100-hPa monthly mean temperatures, states that air is dehydrated during ascent over the fountain region. However, *Sherwood* [2000], based on 14 years (1985–1998) of sonde data, revealed that there is a downward motion at 85 hPa over the maritime continent in boreal winter and proposed a contrasting ''stratospheric drain'' hypothesis. *Hatsushika and Yamazaki* [2001] also successfully reproduced this downward motion using an atmospheric general circulation model (AGCM) driven by observed sea surface temperatures (SSTs) over 44 years. Thus the fountain hypothesis does not hold for the time-

0148-0227/03/2002JD002986$09.00

averaged vertical motion over the maritime continent, and stratospheric dryness requires another explanation.

[3] *Sherwood* [2000] examined the heat budget near the tropopause and found that the budget is not balanced by large-scale processes and radiative heating, suggesting that subgrid-scale convective overshoot and subsequent irreversible mixing of cold air is responsible for cooling of the tropopause layer over Indonesia. *Sherwood and Dessler* [2000] developed and discussed the idea of convective overshoot for dehydration and entry of water vapor into the stratosphere based on observations. *Sherwood and Dessler* [2001] further developed a simple model in which overshooting convective turrets inject dehydrated tropospheric air into a tropical tropopause layer (TTL). They found that for reasonable parameter settings, the combined action of convection, isentropic mixing, and advection by large-scale circulation can reproduce a realistic water vapor profile, although the model is sensitive to the mixing height distribution of the overshoot. Despite these studies, the roles of subgrid-scale convective overshoot and large-scales processes in the stratospheric drain and dehydration remain unclear. The AGCM study by *Hatsushika and Yamazaki* [2001] successfully simulated the drain without the convective overshooting, indicating the possibility that large-scale processes may in fact the dominant cause of the drain. In this study, the structure of vertical motion in the TTL is examined based on AGCM simulation and the factors responsible for the profile are discussed.

[4] *Fujiwara et al.* [1998, 2001] suggested from an analysis of ozone sonde observations over Indonesia and the eastern Pacific that traveling Kelvin waves may be one of the main agents of the troposphere-stratosphere exchange in the tropics. They also suggested that transport by Kelvin waves is one of the main causes of stratospheric dryness.

[5] *Gettelman et al.* [2000] simulated the distribution of water vapor in the upper troposphere and lower stratosphere using a three-dimensional chemical transport model with assimilated winds. They examined vertical moisture flux in an Eulerian framework and found that water vapor enters the stratosphere at all longitudes in the tropics. They also found that detailed subgrid-scale dynamics and convective processes are not needed to explain the entry of water vapor into the stratosphere. *Holton and Gettelman* [2001] proposed the "cold trap" hypothesis and emphasized horizontal transport via a cold trap region. They showed in their two-dimensional (longitude-height) idealized model that significant dehydration occurs in the cold region if horizontally uniform easterly flow prevails in the TTL. *Gettelman et al.* [2002] calculated the water vapor mixing ratio (VMR) using a simple microphysical model with 10-day backward trajectories based on data from the European Centre for Medium-Range Weather Forecasts (ECMWF) and confirmed the relationship between the strong convection over and south of Indonesia and the small water vapor concentration over the Philippines in boreal winter [e.g., *Randel et al.*, 2001]. *Jackson et al.* [2001] diagnosed transport in the tropical tropopause zone in winter using particle trajectories with the ECMWF reanalysis data. They studied forward and backward trajectories from four convective regions, and showed that most trajectories reaching the stratosphere from the lower troposphere cross the tropopause zone over the west Pacific warm pool. This preferred location moves east in an El Niño year and west in a La Niña year. The present study is also based on trajectories, but here show the trajectories themselves to provide a clear Lagrangian view of the circulation and dehydration process in the TTL. The role of transient disturbances such as Kelvin waves in dehydration is also examined.

[6] Several mechanisms of dehydration and entry into the stratosphere have been proposed to date [e.g., *Sherwood and Dessler*, 2000]. However, the contribution of each mechanism remains unclear and is currently under debate. In this study, the capacity of large-scale mechanisms alone to explain the stratospheric drain, dehydration process and entry into the TTL and stratosphere is investigated. The interannual variation in the mixing ratio of water vapor entering the tropical lower stratosphere is also discussed in consideration of the ENSO.

2. Data and Analysis Method

[7] The AGCM used in this study was developed by the Center for Climate System Research/National Institute for Environmental Studies (CCSR/NIES) [*Numaguti et al.*, 1995]. The T42L50 version of the model (1000-0.4 hPa) is used to obtain better vertical resolution in the TTL (700-m resolution from the upper troposphere to the middle stratosphere). Parameterizations for radiation [*Nakajima et al.*, 1995], cumulus convection [*Arakawa and Schubert*, 1974; *Moorthi and Suarez*, 1992] and cloud water [*Le Treut and Li*, 1991] and other standard physical processes are included in the model. The convective overshoot mechanism is not incorporated in the model. The performance of the model with respect to the tropical tropopause structure and its interannual variation with the ENSO has been shown by *Hatsushika and Yamazaki* [2001] based on a 44-year simulation using the observed SST. For a comparison of the simulation with observations, ECMWF objective analysis data (Basic level III consolidated data) for 3 recent years 2000–2002 is used.

[8] For trajectory calculation, new simulations are performed using a composite SST after a 6-year spin-up with the climatological SSTs. The SST data used in this study is monthly mean UK Meteorological Office global ice coverage and sea surface temperature (GISST) data. The SST cycle is prepared in El Niño year and La Niña year patterns by calculating the composite from previous to next boreal wintertime peaks of the SST anomaly in the Niño3 region. The definition of El Niño and La Niña years is as prescribed by the Japan Meteorological Agency. The El Niño years are 1951/52, 57/58, 63/64, 65/66, 68/69, 72/73, 76/77, 82/83, 86/87, 91/92 and 97/98, and the La Niña years are 1954/55, 64/65, 67/68, 70/71, 73/74, 74/75, 84/85, 88/89 and 98/99. The output data is averaged over 3-hour periods and obtained for the same time interval. The averaged data is used in trajectory calculation to avoid spurious vertical diffusion due to very high-frequency waves.

[9] Trajectories are calculated in order to determine how and from where the air in the troposphere is advected into the stratosphere through the TTL. A large number of parcels are allocated either in the troposphere for forward trajectory analysis or in the TTL and above the TTL for backward trajectory analysis. The interval of each parcel in the horizontal direction is 2.5×2.5 for the unsteady state

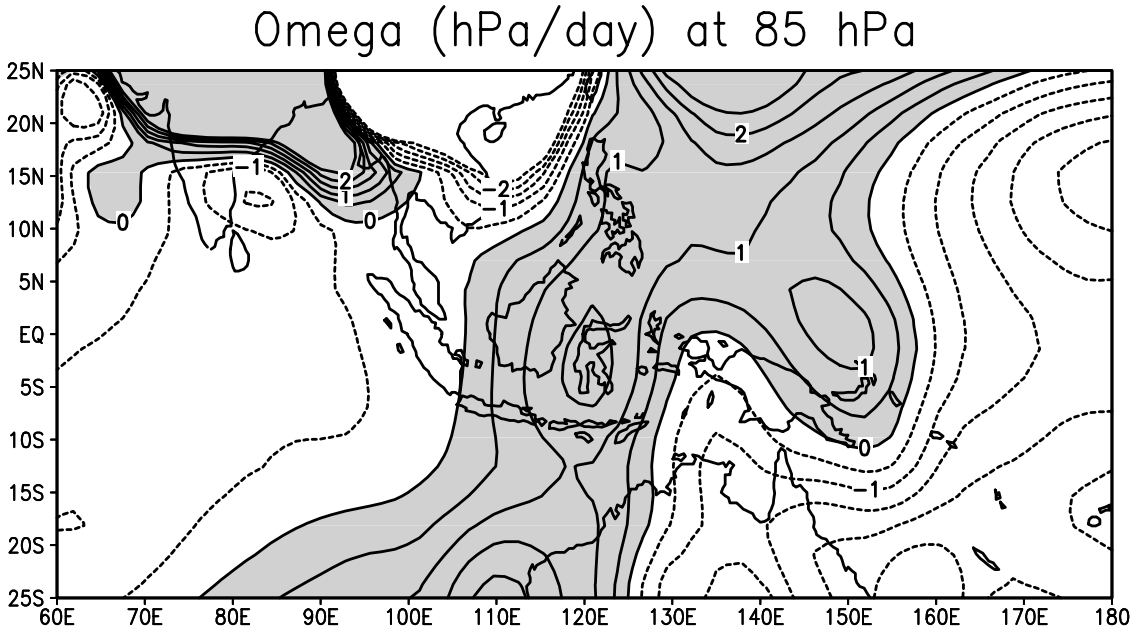

Figure 1. Map of the simulated ω at 85 hPa for the December–February (DJF) season of 1985–1998. Solid contours indicate descent, and dashed contours indicate ascent; the contour interval is 0.5 hPa/day, and contours greater (less) than 3 (−3) hPa/day are not drawn. A nine-point smoothing is applied in zonal and meridional directions. Shaded areas are greater than zero (descent).

experiment, and 1.0 × 1.0 for the steady state experiment. In the forward calculation, parcels are set between 175 and 1000 hPa with a 25-hPa interval. In the backward calculation, the parcels are set from 60 to 150 hPa with a 5-hPa interval. The parcel is transported by the three-dimensional wind field of the AGCM output. The time step of this calculation is 20 min and the trajectories are calculated for a period of 30 days. Linear interpolation is employed in the temporal and horizontal directions, and spline interpolation is adopted for the vertical direction. In this experiment, the model year is 360 days, and each month consists of 30 days. Each 30-day trajectory calculation starts on 1 December, 6 December, 11 December, and so on. In total, 13 cases are calculated. The minimum saturation mixing ratio of water vapor (SMR) along the parcel's path and its location are recorded for each trajectory. The SMR formula is the same as that used in the ECMWF model [*Simmons et al.*, 1999]. It is implicitly assumed that water vapor is transferred to the ice phase when the air is saturated, and that the ice falls out immediately. As recent measurements have shown that supersaturation occurs frequently [e.g., *Jensen et al.*, 1999] and the critical relative humidity might be higher than 100%, the present assumption underestimates the stratospheric VMR. However, this does not affect the results qualitatively because the VMR varies linearly with the critical relative humidity.

3. Causes of Downward Motion Over the Maritime Continent

[10] The simulated vertical p velocity (ω) at 85 hPa for the December–February (DJF) season of 1985–1998 is shown in Figure 1 (see also Figure 4 in *Hatsushika and Yamazaki* [2001]). This period was chosen to allow comparison with the results of *Sherwood* [2000]. The pattern is similar to that obtained from sonde analysis by *Sherwood* [2000] and also similar to that obtained from the ECMWF analyses by *Simmons et al.* [1999]. The present simulation reveals a downward velocity of about 1 hPa/day over Indonesia and upward velocity over the western and central Pacific, consistent with observations.

[11] The cause of the downward motion around the tropopause over the maritime continent is examined by heat budget analysis, as conducted by *Sherwood* [2000]. Figure 2 shows the vertical profile of the heat budget over the maritime continent (105–125°E, 5°S–5°N; thick line) and the western Pacific (160°–180°E, 5°S–5°N; thin line). Adiabatic heating associated with the downward motion $(-\bar{\omega}\frac{\partial\theta}{\partial p})$ is primarily balanced by horizontal cold advection $(-\bar{\mathbf{v}}\cdot\nabla\theta)$ over the maritime continent. A small residual is balanced by minor diabatic heating. Over the western Pacific (thin line), the adiabatic cooling by upward motion is balanced largely by horizontal warm advection and additionally by diabatic heating. The downward motion therefore appears to be caused by a dynamical process over the maritime continent. The same result has been obtained using an aqua planet simulation with a rectangular warm water pool in the equatorial region [*Hatsushika*, 2001].

[12] In the work of *Sherwood* [2000], cold horizontal advection is almost zero and the heat budget is not balanced. To explain this, it was suggested that cumulus overshoot unresolvable by the sonde network causes cooling. However, the cold horizontal advection in the work of *Sherwood* [2000] may be underestimated due to the sparsity of sonde stations over the western equatorial Pacific (upstream of the maritime continent), although overshoot may indeed contribute to cooling to some extent in the real atmosphere.

[13] It is noted that diabatic heating is weak over the maritime continent compared with that over the western Pacific. This difference is attributed to the difference in

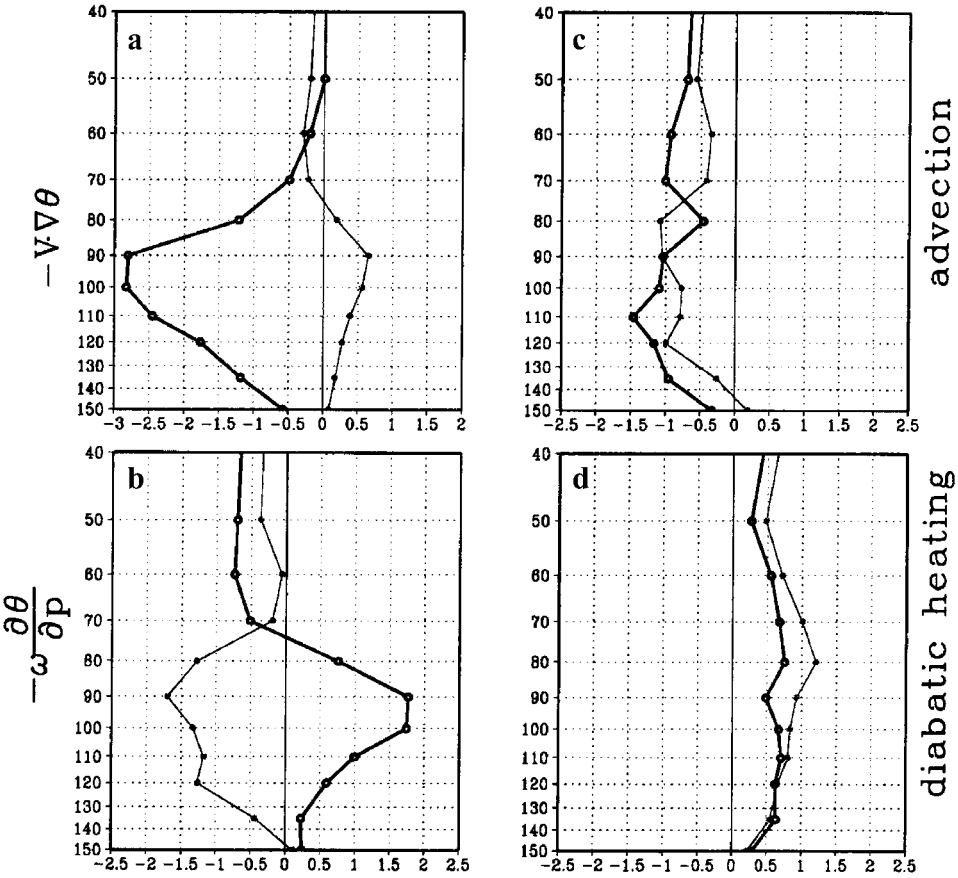

Figure 2. Composite profiles of the heat budget: (a) horizontal heat advection, (b) vertical heat advection, (c) total advection, and (d) diabatic heating. The thick line denotes the average over the maritime continent (105°–125°E, 5°S–5°N). The thin line denotes the average over the western Pacific (160°–180°E, 5°S–5°N). The unit is K/day.

longwave heating. Shortwave heating is almost the same over the two regions, and convective heating is zero above 110 hPa. Over a deep convection region, the cold cloud top radiates a minor amount of longwave radiation upward in comparison to clear regions, where the warm SST radiates a large amount of upward longwave radiation. Thus the absorption of longwave radiation is reduced over convective regions. Weak or negative diabatic heating at 70 hPa over convective regions is also indicated in ECMWF data [*Norton*, 2001]. Reduction of longwave heating over deep convection suppresses upward motion over the maritime continent.

[14] To examine the dynamic process in more detail, the potential temperature and zonal and upward wind near the equator (averaged between 5°S and 5°N) for La Niña years are shown in Figure 3a. The upward motion and low potential temperature region lies over the convective region between 100°E and 150°E at 150 hPa. This is caused mainly by active convection. Around the tropopause, the cold region tilts eastward with height, probably representing a steady Kelvin wave response to convective heating below. The coldest region shifts eastward to 150°–160°E at 100 hPa, and around the dateline at 70 hPa. Thus the isentropic surface declines toward the west over the maritime continent, and the easterly (westward) wind in that region causes downward motion when the flow is adiabatic. The westward flow over the eastward tilting upward bulge of the isentrope explains the downward motion over strong convective areas in terms of pressure coordinates. The same plot for a recent 3-year period (2000–2002) of the ECMWF analysis is shown in Figure 3b. Similar features can be seen, although the ECMWF data exhibits only 3 levels around the tropopause, i.e., 150, 100, and 70 hPa.

4. Results of Trajectory Calculations

[15] The AGCM simulated the spatial patterns of the tropopause temperature and vertical velocity around the tropopause in the tropics well, although the model contains a uniform cold bias of about 4 K [*Hatsushika and Yamazaki*, 2001]. The simulated lapse rate tropopause is about 93 hPa, and the potential temperature of the tropopause is about 375 K in the tropics. From trajectory calculations, the cross-TTL parcels starting below a potential temperature of 350 K and ending above 390 K are selected, roughly corresponding to the lower and upper boundaries of the TTL [*Highwood and Hoskins*, 1998].

[16] To examine the origin of the air parcels that reached the stratosphere, Figure 4 shows the number densities of the initial locations of air that entered the stratosphere (top) and the longitude-pressure cross sections (bottom). Most of the parcels originate from over the maritime continent and

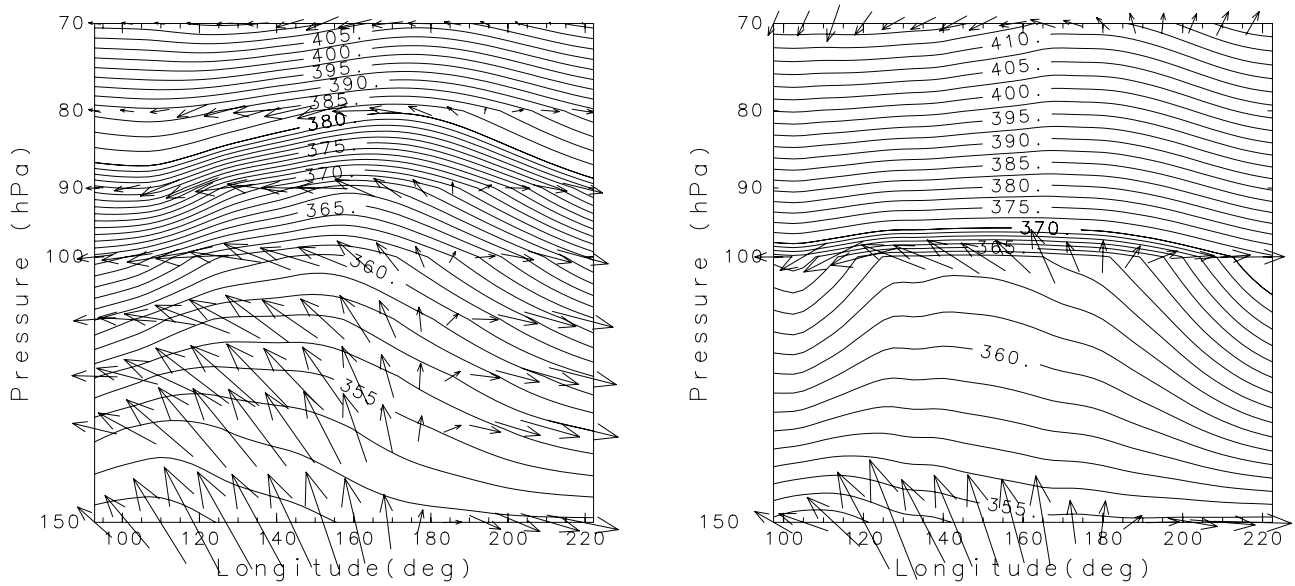

Figure 3. (left) Longitude-pressure cross section for potential temperature (contour), vertical p velocity, and zonal wind (arrow) for La Niña composite. The length of the arrow is expressed as a 1 day path. (right) Same as in Figure 3 (left) but for the European Centre for Medium-Range Weather Forecasts analysis for DJF 2000–2002.

tropical western Pacific (i.e., the stratospheric fountain region) in the La Niña experiment, corresponding to the active convective region in La Niña years. In El Niño years, the area extends eastward responding to the eastward shift of convection. Over 70% of the air parcels that entered the stratosphere originate from the stratospheric fountain region. The other two minor regions are located over South Africa and South America, as well as convective regions. The centers of these three regions are situated south of the equator.

[17] For analysis of the minimum SMR locations, the number densities are shown in Figure 5. The parcels that entered the TTL from three convective regions exhibit minimum SMRs around the stratospheric fountain region in their trajectories. The southward displacement from the equator is moderated in both of the top panels of Figure 5 by

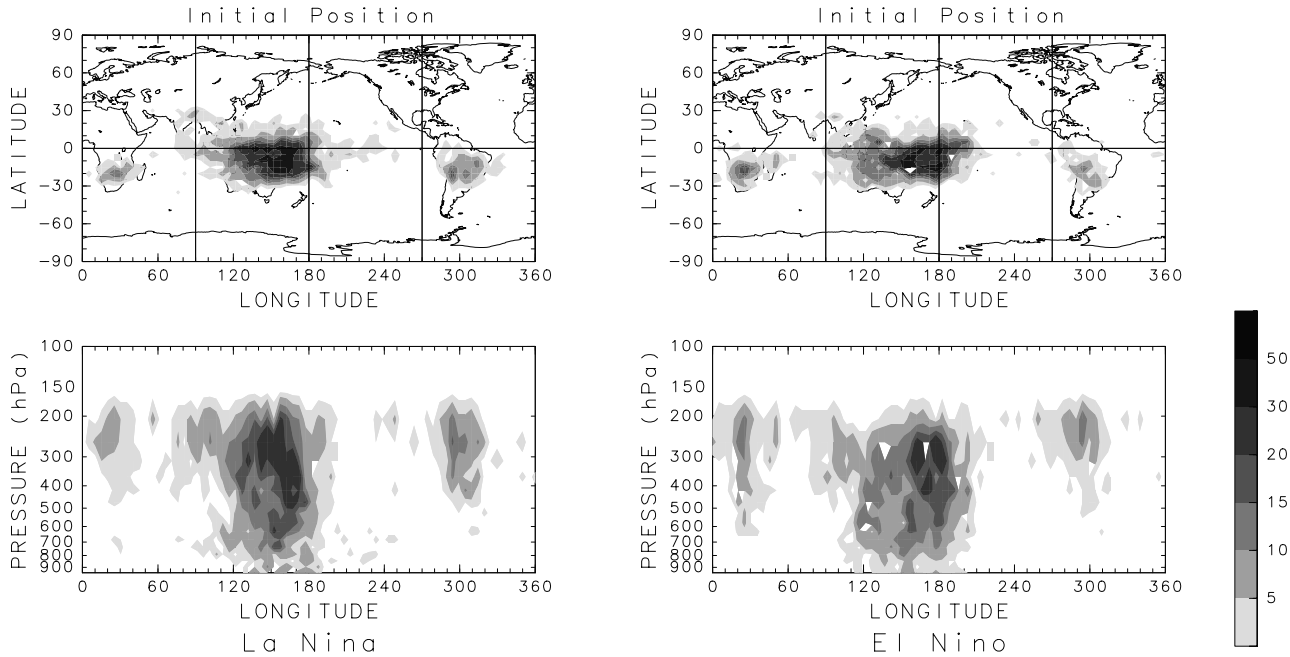

Figure 4. (top) Horizontal maps and (bottom) longitude-pressure cross sections of number densities for the parcels' initial locations. Parcels starting below $\theta = 350$ K and ending above $\theta = 390$ K are counted. Darker colors denote larger number densities. (left) La Niña years. (right) El Niño years.

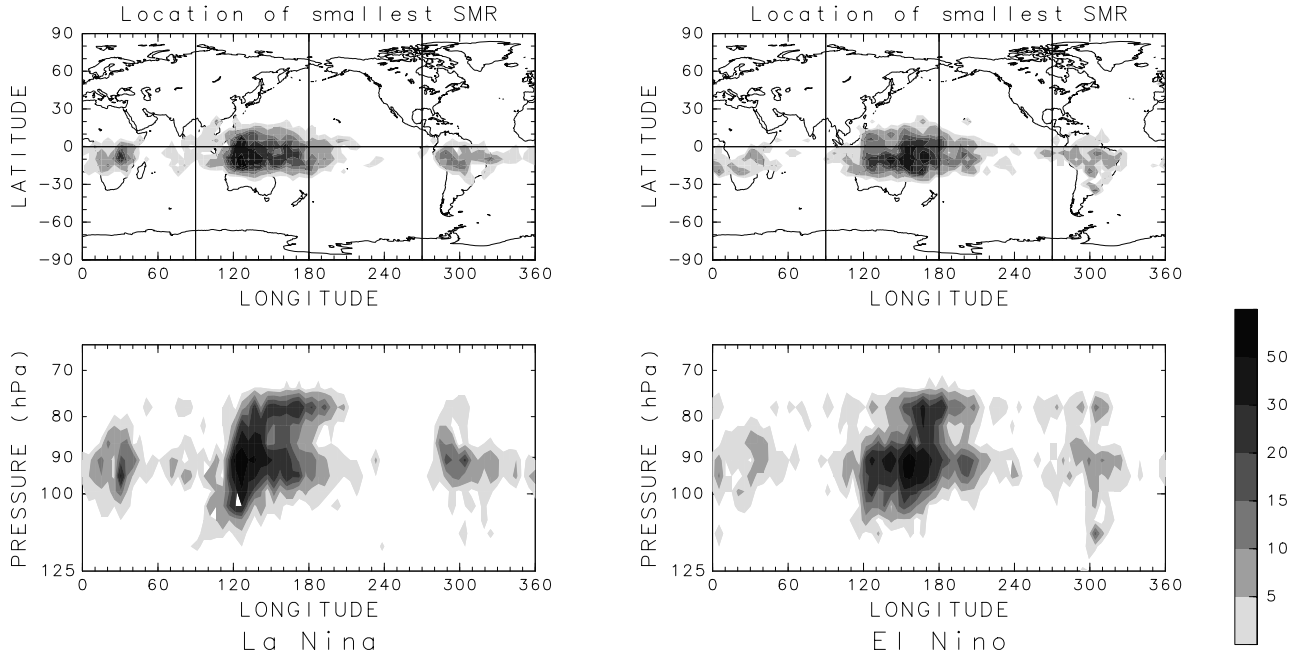

Figure 5. (top) Horizontal maps and (bottom) longitude-pressure cross sections of number density for the parcels' minimum saturation mixing ratio of water vapor (SMR) locations. Parcels starting below θ = 350 K and ending above θ = 390 K are counted. Darker colors denote larger number densities. (left) La Niña years. (right) El Niño years.

the symmetry of the cold tropopause region about the equator [e.g., *Randel et al.*, 2001; *Hatsushika and Yamazaki*, 2001] (see also Figure 6 in this paper).

[18] These results are consistent with the stratospheric fountain hypothesis in that air passes the fountain region on the way to the stratosphere. However, the air does not readily ascend directly to the stratosphere in this region because the mean vertical motion around the tropopause is downward [*Sherwood*, 2000; *Hatsushika and Yamazaki*, 2001]. Therefore the term "fountain," indicative of a continuous ascent as *Newell and Gould-Stewart* [1981] hypothesized, does not seem to be appropriate.

[19] Figure 6 shows the equatorial vertical p velocity, zonal wind, and SMR maps around the tropopause. A strong upward motion exists over the fountain region up to 110 hPa. At the bottom of the TTL, the fountain region has by far the strongest upward velocity. It is not surprising that more than two thirds of parcels that entered the stratosphere originate from this region. The strong convection yields the Matsuno-Gill pattern [*Matsuno*, 1966; *Gill*, 1980], a pair of anticyclonic cells straddling the equator and westerly wind to the east along the equator, as shown in middle and bottom maps of Figure 6. The ECMWF data also reveals a pair of anticyclones at 100 hPa. The air over the maritime continent and the western Pacific in the lower TTL will be transported westward by prevailing easterlies in that area. As the vertical velocity between 100 hPa and 80 hPa is downward, as shown in the top right plot of Figure 3, the air would not be dehydrated efficiently and would not enter the stratosphere directly soon after entering the TTL if the air is transported by flow in the height-longitude cross section (Figure 6). Simple westward horizontal transport [*Holton and Gettelman*, 2001] does not seem to provide effective dehydration.

[20] Trajectories of cross-TTL air parcels in the La Niña January experiment are shown in Figure 7, with the corresponding SMRs denoted in color. Figure 7 shows air parcels with initial potential temperatures of less than 350 K and final potential temperatures of more than 390 K. From Figure 7a, it can be seen that parcels that entered the TTL originated mostly from the troposphere in the fountain region. From Figure 7b, it is noted that the main initial locations are in the Southern Hemisphere (see below 200 hPa), corresponding to active convective regions. However, the trajectory distribution is rather symmetric about the equator in the TTL. The parcels are gradually dehydrated around the equator during the ascent to the stratosphere. The dehydrated air around the tropopause level is dispersed widely to other longitudes and latitudes, but remains largely concentrated over the fountain region. These results are consistent with *Jackson et al.* [2001].

[21] Figure 7c, showing horizontal trajectories, reveals again that the trajectories are mainly concentrated over the fountain region. There are also many westward trajectories near the equator. Further, it is noted that the parcels seem to rotate over the three convective regions, particularly over the fountain region. This point is discussed in the next section.

[22] Backward trajectories from the levels above the TTL indicate that entry into the stratosphere from the TTL is quite uniformly distributed (figures not shown). This is in accordance with *Gettelman et al.* [2000], and demonstrates that the condition at the top of the TTL is not consistent with the stratospheric fountain model.

5. Transport by Steady Flow

[23] It was shown in the previous section that the cross-TTL parcels are affected by anticyclones over the three

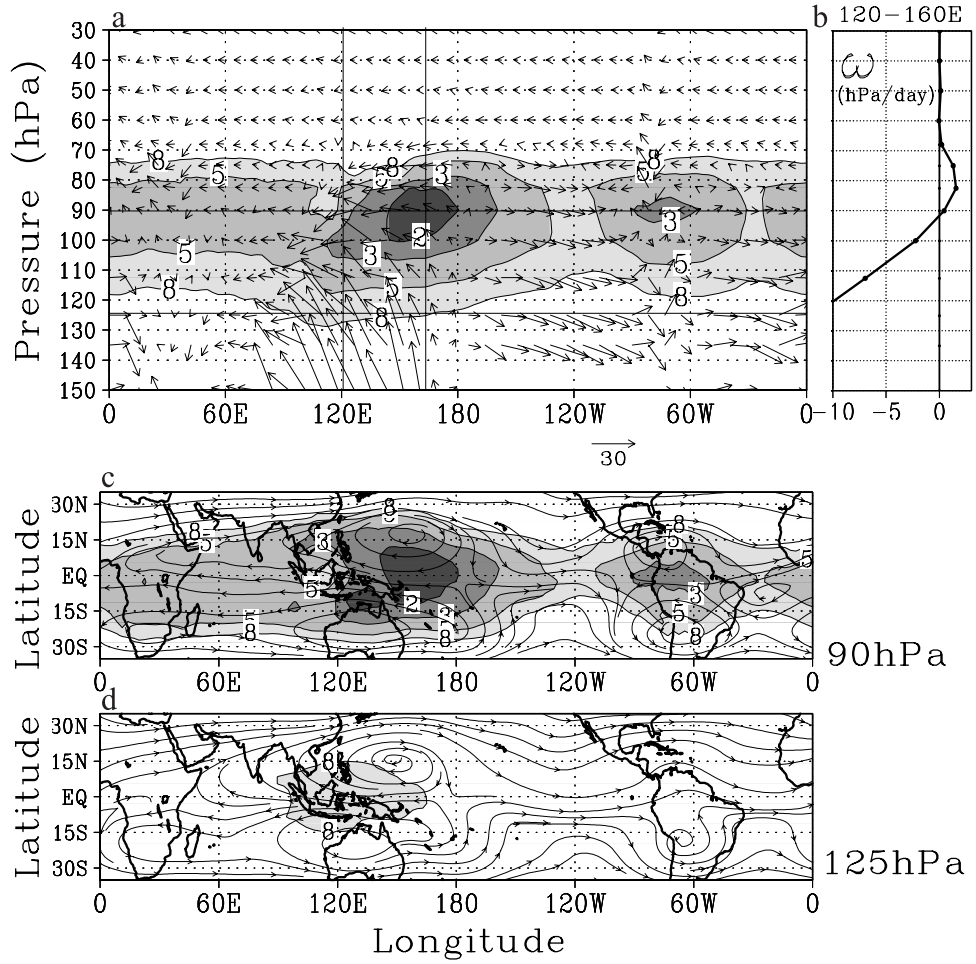

Figure 6. (a) Longitude-pressure cross section of wind and SMR averaged over the equatorial latitudes (10°S–10°N). SMRs less than 2, 3, 5, and 8 ppmv are shaded. (b) Vertical profile of ω averaged over the region between 120°E and 160°E. The unit is hPa/day. A vertical range of from 150 hPa to 30 hPa is shown in each panel. (c) Horizontal map of streamlines at 90 hPa and the SMR. The region between 35°S and 35°N is shown. (d) The same as in Figure 6c but for 125 hPa.

convective regions. To idealize this model, trajectories are calculated using DJF mean fields under the La Niña condition. In this case, the upper limit of potential temperature is lowered to 385 K because few parcels reached more than 390 K after 1 month.

[24] Figure 8 shows the trajectories of air parcels transported by steady mean flow. Anticyclonic trajectories are seen over the western Pacific, South Africa and South America. The parcels gradually ascend and circle around the anticyclone in a spiral movement. The parcels traverse across the cold region near the equator every rotation. Thus the rotating parcels enter the cold region many times, where they are dehydrated. The radius of rotation gradually increases due to divergent flow associated with anticyclones. Over Australia, many parcels were ejected to the west after several rotations.

[25] There are no trajectories in the Northern Hemisphere (NH) in Figure 8c because the upward velocity in the NH is smaller than in the Southern Hemisphere (SH). If the potential temperature limit is set to 350–375 K, many trajectories show up in the Northern Hemisphere. The bottom of Figure 8 shows such trajectories for January mean flow. Some trajectories start from the SH and circle around the SH anticyclone, cross the equator and circle around the NH anticyclone. These trajectories reflect the local Hadley circulation and contribute to shifting the water vapor minimum into the winter hemisphere [*Gettelman et al.*, 2002]. As the diabatic heating rate in the TTL is 0.5–1.0 K/day in terms of potential temperature (see Figure 2), it takes 25 to 50 days for a parcel to increase its potential temperature by 25 K. The behavior of trajectories in Figure 8 is consistent with the heating rate.

[26] On the basis of this analysis, a new dehydration mechanism is proposed, as schematically illustrated in Figure 9. The air is transported into the TTL by strong ascent resulting from local strong convection. The main entry into the TTL occurs over Indonesia and the western Pacific, corresponding exactly with the stratospheric fountain region. This region is a fountain at the bottom of the TTL, but not at the top. After entering the TTL, many parcels are entrained into anticyclonic cells and become dehydrated in the cold region near the equator. This cold trap works repeatedly. Within the TTL, parcels travel all longitudes, but once air passes the cold fountain region near

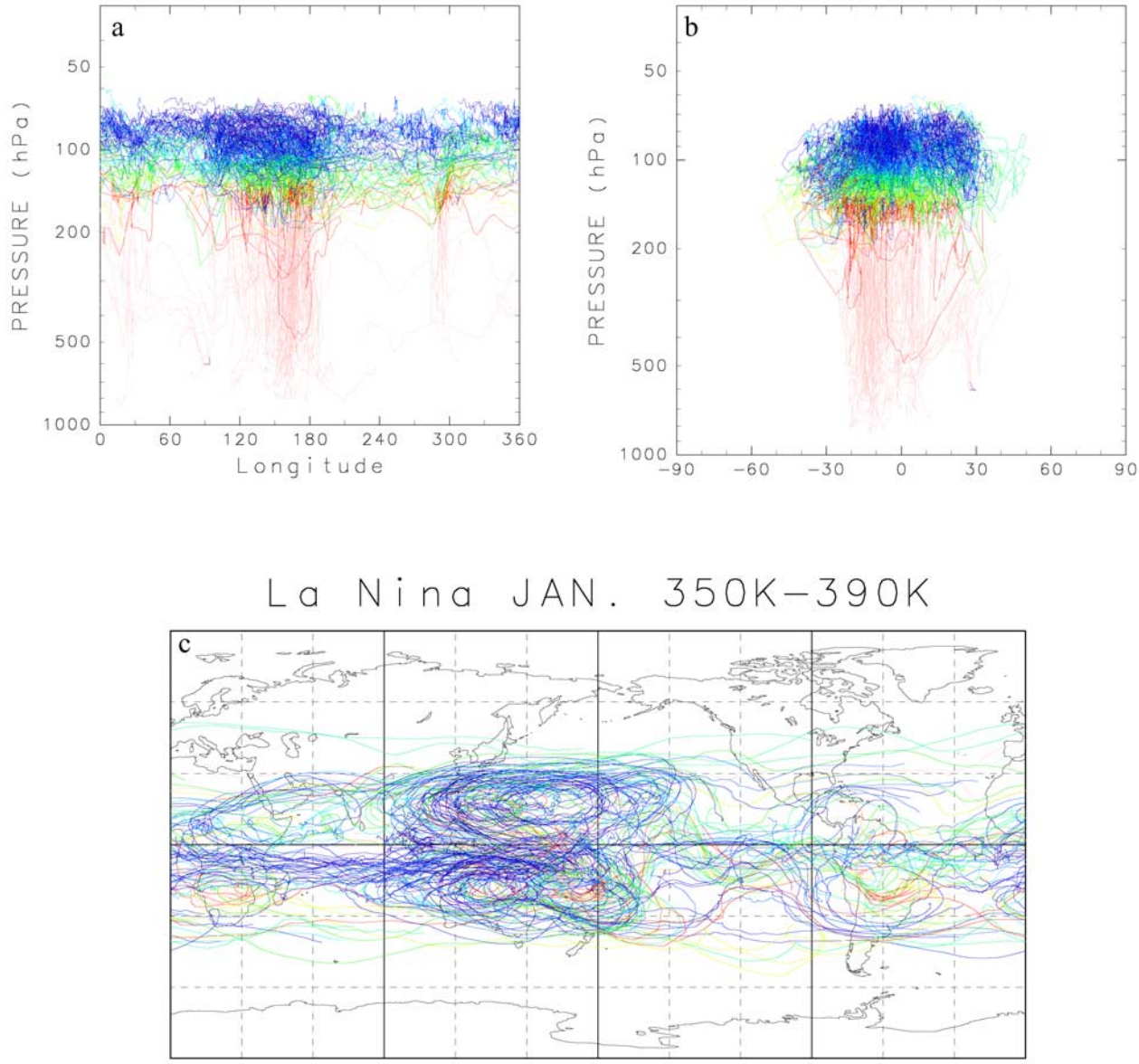

Figure 7. Trajectories of cross-tropical tropopause layer air in the La Niña January experiment in (a) a longitude-pressure cross section, in (b) a latitude-pressure cross section, and in (c) a horizontal plane. Parcels starting below $\theta = 350$ K and ending above $\theta = 390$ K are drawn. The color denotes the parcel's water vapor mixing ratio (VMR) (warmer colors indicate a larger VMR).

the equator, the air is dehydrated, ascends across the top of the TTL more uniformly.

6. Role of Disturbances to the Stratospheric VMR

[27] Comparison of Figure 7 (with time-varying wind) and Figure 8 (with steady wind) reveals that transience causes stochastic transport from the troposphere to the stratosphere. It can also be seen that the mean SMR in the temporally varying experiment is smaller than that in the steady wind experiment.

[28] To see the importance of transience in the development of the stratospheric dryness, Figure 10 shows the standard deviation (SD) of vertical p velocity, zonal wind, meridional wind and variations of temperature and SMR at 90 hPa in the equatorial region (10°N–10°S) for the La Niña experiment. In general, the SD of vertical velocity is much larger than the mean value itself and the SD is large over the three convective regions, especially over the fountain region. In the upward phase of large disturbances, water vapor is condensed and transported into the stratosphere with small VMR due to adiabatic cooling, whereas during the downward phase, water vapor is simply transported downward. The intermittent upward motion therefore represents an effective dehydration process. The zonal wind (Figure 10b) exhibits large perturbations to the west of the fountain region, while the SD of the meridional wind (Figure 10c) peaks over the eastern Pacific. The minimum

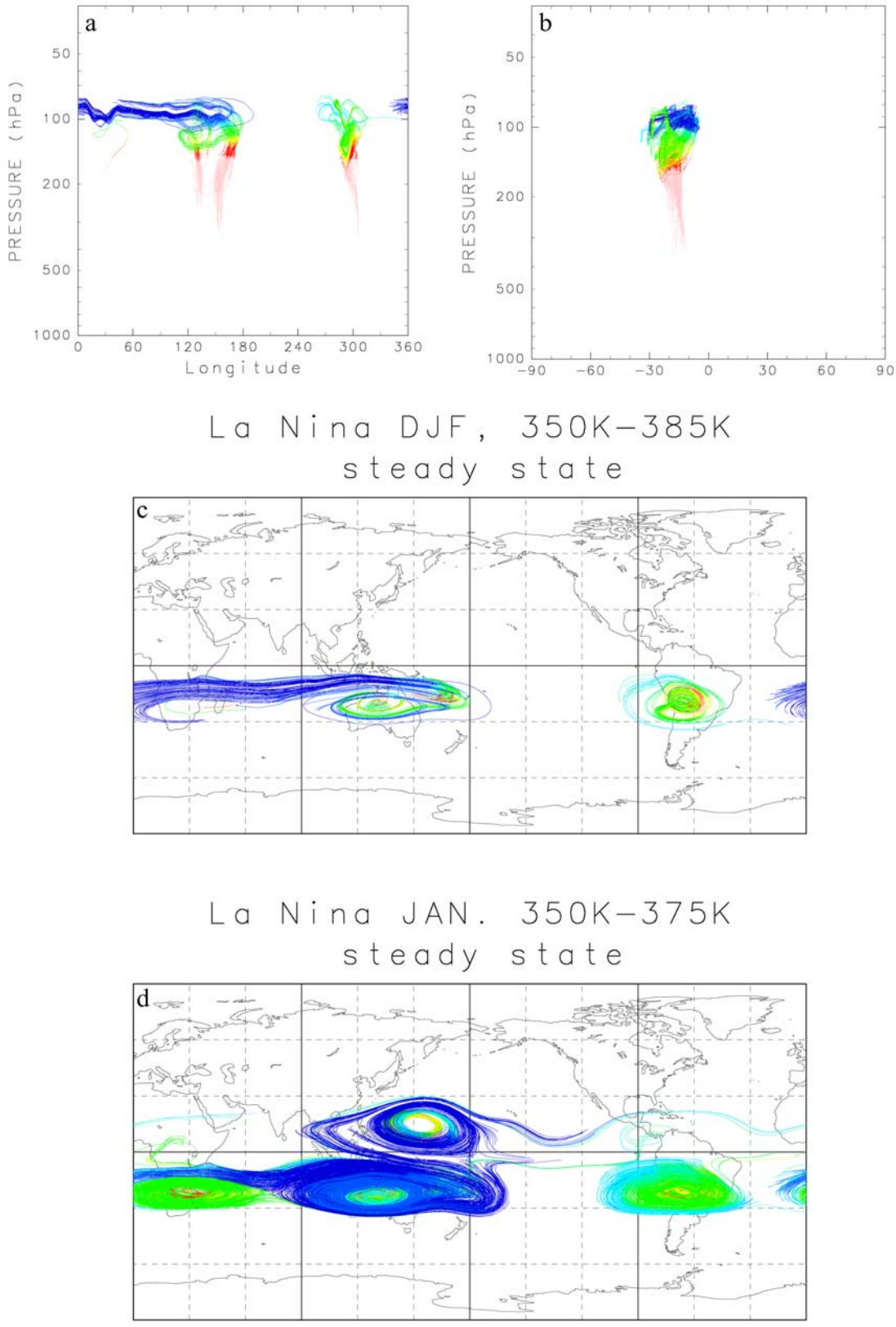

Figure 8. (a–c) Same as in Figure 7, except for the DJF mean state condition, and the critical final potential temperature is set as 350–385 K. (d) January mean state condition; the critical final potential temperature is set as 350–375 K.

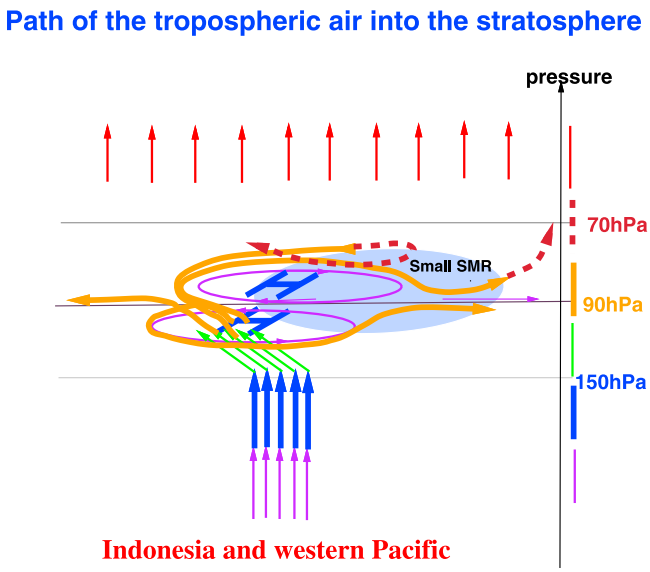

Figure 9. Schematic picture for the path of the air from the troposphere to the stratosphere through the tropical tropopause layer. The color of each line denotes the pressure level, and the shaded area corresponds to the minimum SMR region. The anticyclones around the tropopause are also drawn with purple lines.

mean temperature is located around 150°E (Figure 10d). The large SD of vertical p velocity in the region 120°–150°E give rise to a flat mean minus SD temperature in this area. Zonal advection appears to produce a large SD of temperature around 120°E, where the zonal gradient of temperature is large. The variation in SMR (Figure 10e) follows the change in temperature exponentially, and is affected by the SDs of temperature and mean temperature. The minimum SMR (mean minus SD) is seen not at the smallest mean SMR but to the west of it. Thus the lowest SMR (mean minus SD) of less than 1.5 ppmv is located over the region 120°–180°E, which corresponds well to the distribution in Figure 5 (left panels). These results roughly agree with the ECMWF data at 100 hPa for the 2000–2002 winter seasons (shown by thin lines), although the temperature and SMR minima in the ECMWF data are less conclusive.

[29] To investigate the respective contributions of low-frequency variations such as Kelvin waves or intraseasonal oscillation and high-frequency variations such as gravity waves to lower stratospheric dryness, each of the wind and temperature fields in the La Niña experiment were divided into low-frequency disturbances and high-frequency disturbances. The low-pass filtered temperature and wind fields were calculated by smoothing the field of the standard experiment using a 7-day running mean, and the high-pass filtered field was obtained by adding the residual of the low-pass filter to the 30-day mean field. The variance in the low-frequency disturbance is smaller than that of the high-frequency disturbance in terms of ω and V, but approximately the same for U (Figures 11 and 12). The disturbance of ω over the maritime continent prevails in the high-pass filtered experiment (Figure 12a), more so than in the low-pass filtered experiment (Figure 11a). However, the high-pass filtered ω variance is zonally uniform compared to the low-pass filtered results. The longitudinal variations of U and V variances in Figures 10b and 10c are dominated by the low-frequency perturbations (Figures 11b and 11c). Although the magnitudes of the temperature and SMR variances are generally larger in the high-pass filtered fields, the longitudinal variations are larger in the low-pass filtered fields.

[30] Using these fields, 30-day trajectories for the La Niña experiment and the El Niño experiment were calculated, recording the minimum SMR for each parcel. Figure 13 shows the number of air parcels reaching the stratosphere and the mean SMR of each experiment for the low-frequency, high-frequency, and standard experiments. The high-frequency perturbations transport more air parcels to the stratosphere effectively. However, the acquired VMR is large, which means that the high-frequency variations such

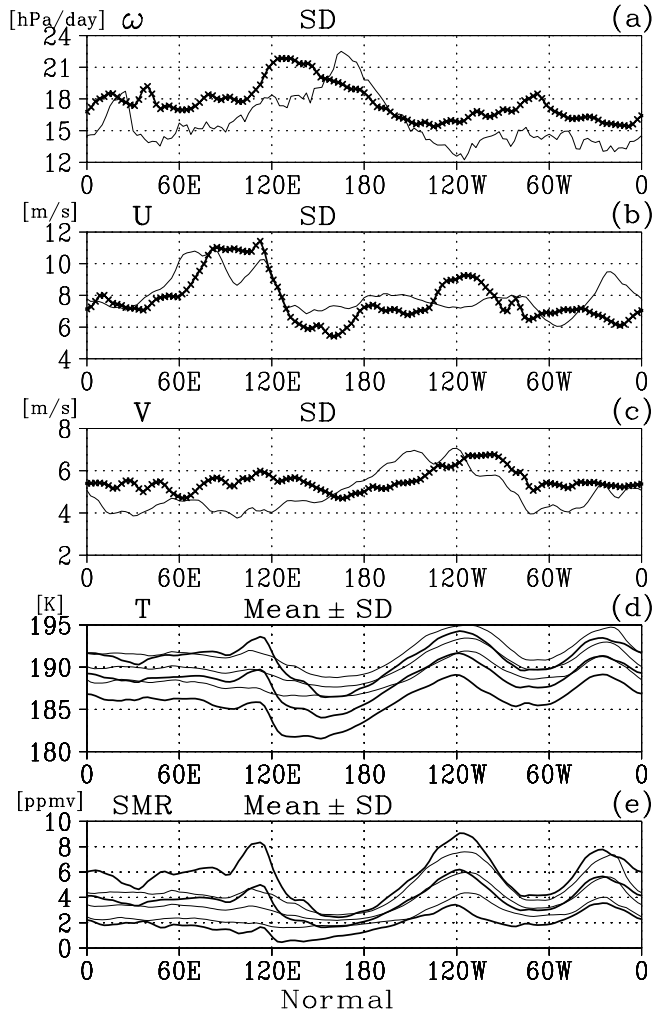

Figure 10. Standard deviations (SDs) of (a) the vertical p velocity (ω), (b) zonal wind (U), (c) meridional wind (V), (d) temperature, and (e) SMR in the equatorial region at 90 hPa. Data in the La Niña experiment is averaged from 10°S to 10°N. For Figures 10d and 10e, the mean, the mean plus SD, and the mean minus SD are drawn. Observed data based on the ECMWF analysis for 2000–2002 are also drawn (thin lines).

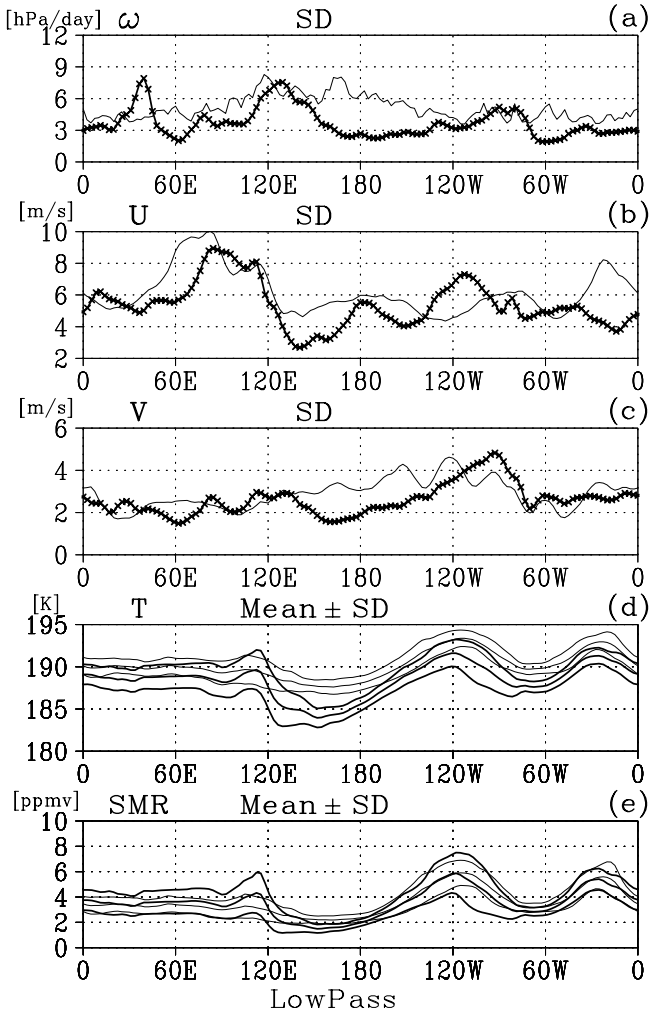

Figure 11. Same as in Figure 10 but for the low-pass filtered experiment.

as gravity waves are not efficient for dehydration of the air in the TTL. This is because the high-frequency disturbances transport air parcels to the stratosphere uniformly in the zonal direction, and some air parcels pass the warmer TTL regions. Thus the mean VMR becomes large. On the other hand, upward transport due to low-frequency disturbances is dominant over the fountain region, resulting in a low mean VMR but not transport much air into the stratosphere. Thus the low-frequency disturbances such as Kelvin waves efficiently dehydrate the air in the TTL. The intermittent upward motion is therefore an important agent in the development of stratospheric dryness. In the standard experiment, the VMR becomes low but the number of parcels remains at intermediate values.

7. Interannual Variation of Water Vapor Associated With ENSO

[31] The interannual variation of the stratospheric water vapor with the ENSO cycle is examined again by calculating the mean SMR and column total number densities in each longitudinal range. This AGCM has a cold bias of about 4 K in the tropopause region compared to observations. Therefore the SMR at the tropopause and estimated stratospheric VMR are lower than observed, by half. However, the difference between El Niño and La Niña years can be discussed qualitatively because the bias is horizontally uniform. The VMR in the equatorial lower stratosphere is determined by the temperature in the coldest region in the tropopause, which shifts longitudinally with the ENSO cycle. *Hatsushika and Yamazaki* [2001] analyzed the AGCM simulation and found that the pattern of vertical motion in the TTL also shifts eastward corresponding to the ENSO cycle. Thus the entry of air parcels and the water vapor into the stratosphere changes with the ENSO cycle.

[32] The initial longitudinal range and smallest SMR of the parcels entering the stratosphere are shown in Figure 14. In the La Niña experiment, the main entry occurs in the longitudinal range of 120°E ∼ 150°E, with secondary entry in the range 150°E ∼ 180°E, and about 44% of parcels are less than 1.0 ppmv. In the El Niño experiment, the main entry shifts eastward to 150°E ∼ 180°E and the ratio of parcels of less than 1.0 ppmv is about 32%. In the El Niño experiment, the mean SMR is 15% higher than in the La Niña experiment, attributed to the warmer minimum tropopause temperature. This feature of interannual variation

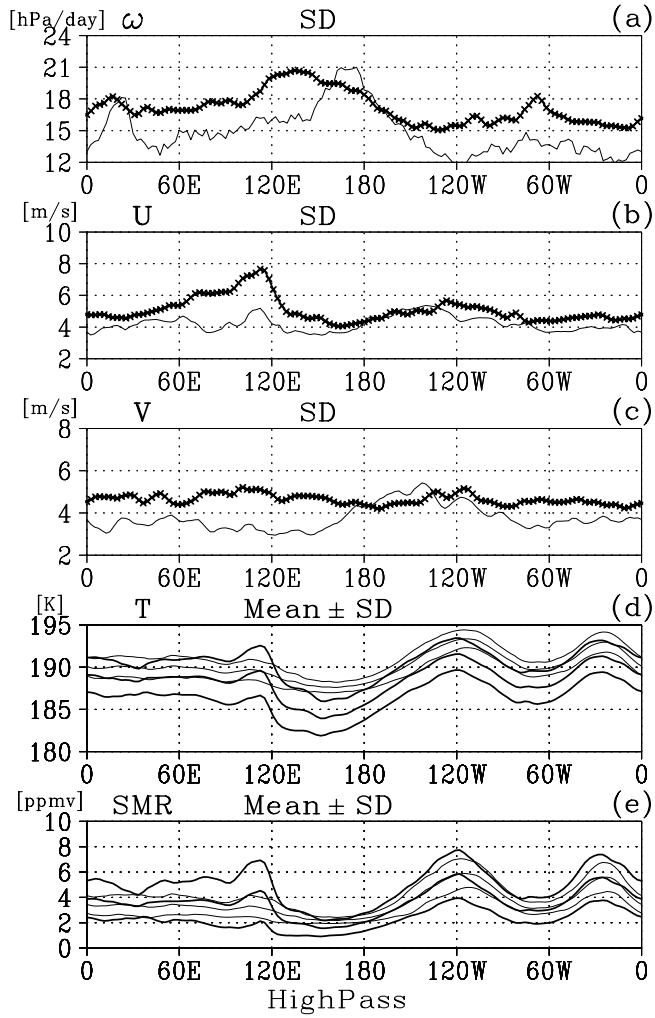

Figure 12. Same as in Figure 10 but for the high-pass filtered experiment.

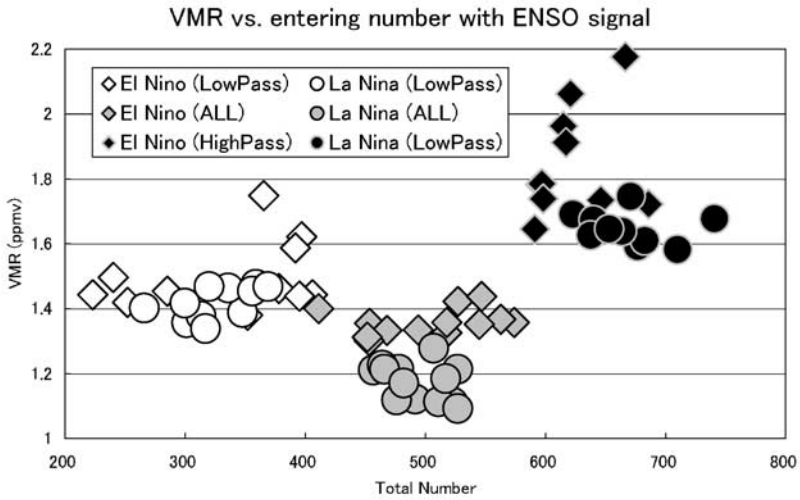

Figure 13. Scatterplot of the total number and mean acquired VMR for the standard, the high-pass filtered, and the low-pass filtered experiments.

of VMR is consistent with the analysis for the 1997/98 winter (El Niño) and for the 1998/99 winter (La Niña) using UARS/HALOE satellite sounding observations [e.g., *Gettelman et al.*, 2001; *Randel et al.*, 2001], although previous analyses did not remove the effect of QBO.

[33] The change associated with the ENSO is large in both the high-pass and standard experiments, and small in the low-pass experiment (Figure 13). As the high-pass disturbances boost air parcels more uniformly, the number of air parcels passing outside the fountain region, where the tropopause temperature is higher, increases in El Niño years. This effect also contributes to the increase in the mean VMR in El Niño years.

8. Summary

[34] The AGCM simulates the temperature structure in the TTL well including downward motion over Indonesia as indicated from sonde observations by *Sherwood* [2000]. Around the tropopause, strong easterlies prevail and the cold ascent region tilts eastward. A down-slope flow over the upward-bulging isentropic surface produces the downward p velocity over Indonesia. Additionally, reduction of longwave heating over deep convection suppresses upward motion. These features of the circulation and temperature structure in the TTL are consistent with the ECMWF analysis. The present results suggest that the stratospheric drain is mainly caused by large-scale dynamic and radiative processes.

[35] The results of trajectory calculation indicate that many air parcels enter the TTL over the maritime continent and the western tropical Pacific in boreal winter. This region is a fountain from the troposphere to the TTL. In the TTL, a pair of anticyclonic flows straddles the equator as a dynamic response of the atmosphere to diabatic heating over the fountain region. This anticyclonic circulation entrains air parcels, which pass the equatorial cold region during the course of spiral ascent. Thus the air parcels pass the equatorial cold region several times along the trajectories and become fully dehydrated, even if the mean vertical motion over the maritime continent is locally downward.

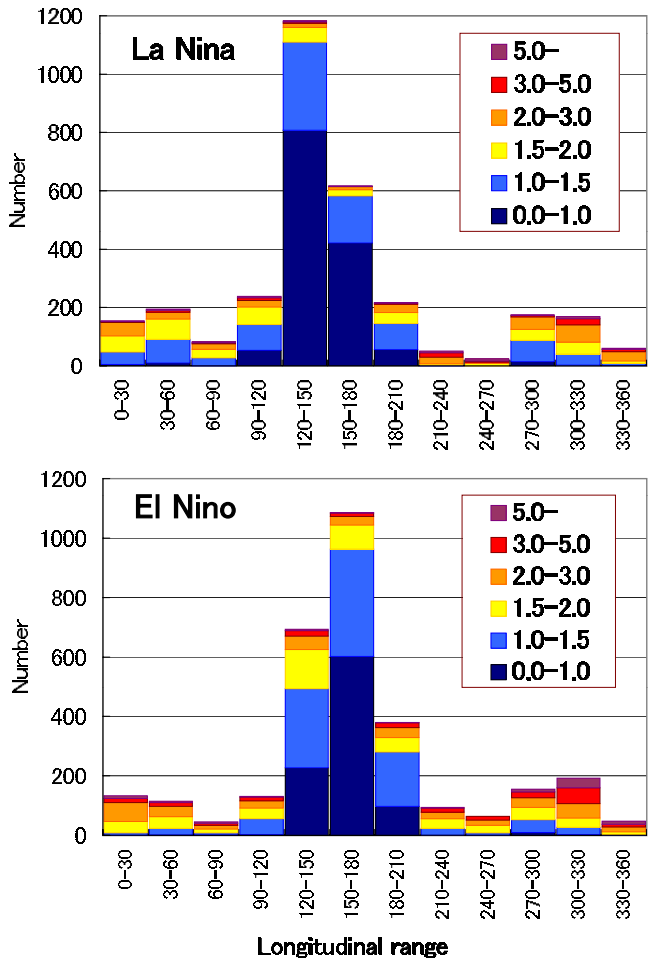

Figure 14. Number of initial locations of parcels that entered the stratosphere and their SMRs for each longitudinal range. (top) La Niña years. (bottom) El Niño years.

Entry of these parcels into the stratosphere is more uniform and ascent is slow across the top of the TTL.

[36] Transient disturbances such as Kelvin waves also play an important role in transport, as well as in dehydrating the air effectively, as suggested by previous studies [*Fujiwara et al.*, 1998, 2001; *Fujiwara and Takahashi*, 2001]. High-frequency transient disturbances such as gravity waves also play a role in troposphere-stratosphere exchange, although the mean stratospheric VMR due to the high-frequency waves is not as low as that due to low-frequency waves. The interaction of high-frequency and low-frequency perturbations fully dehydrates the air.

[37] Changes in the entry structure and stratospheric water vapor with the ENSO cycle were also investigated. The lower stratosphere in the equatorial region should be 15% wetter in the El Niño years. In the zonal mean, the El Niño years are colder than the La Niña years (by 0.6 K in DJF and 0.8 K in JJA from NCEP data), although the minimum temperature is higher. It has been suggested that the VMR in the lower equatorial stratosphere is mainly controlled by the minimum temperature of the coldest region. Thus, since the frequency of the El Niño over the last 2 decades has been higher than the previous period, the ENSO effect should be taken into account when considering the interannual variation or trend of the stratospheric VMR [*Evans et al.*, 1998]. Additionally, the high-frequency disturbances also appear to be important for the VMR. The interannual variation and trend of the disturbances may therefore be important factor contributing to the interannual variation of the stratospheric VMR.

[38] In this study, dynamic and longwave heating mechanisms were proposed to explain the mean downward motion over the maritime continent, and spiral motion around a pair of anticyclones was emphasized for its importance in dehydration. According to this dehydration mechanism, the region over Indonesia and the western Pacific is a key area governing the stratospheric water vapor. The AGCM used in this study does not include the convective overshoot observed in the real atmosphere, and the roles of overshoot and subgrid-scale processes in dehydration need to be studied.

[39] **Acknowledgments.** The authors wish to thank the Center for Climate System Research (CCSR), the University of Tokyo, and the National Institute of Environmental Studies (NIES), Japan, for use of the CCSR/NIES GCM. D. V. Bhaskar Rao and two anonymous reviewers are thanked for improving the manuscript. This work was partly funded by a Grant-in-Aid for Scientific Research in Priority Areas (B), No 11219201.

References

Arakawa, A., and W. H. Schubert, Interactions of cumulus cloud ensemble with the large-scale environment, part I, *J. Atmos. Sci.*, *31*, 671–701, 1974.

Evans, S. J., R. Toumi, J. E. Harries, M. P. Chipperfield, and J. M. Russell III, Trends in stratospheric humidity and the sensitivity of ozone to these trends, *J. Geophys. Res.*, *103*(D8), 8715–8725, 1998.

Fujiwara, M., and M. Takahashi, Role of the equatorial Kelvin wave in stratosphere-troposphere exchange in a general circulation model, *J. Geophys. Res.*, *106*(D19), 22,763–22,780, 2001.

Fujiwara, M., K. Kita, and T. Ogawa, Stratosphere-troposphere exchange of ozone associated with the equatorial Kelvin wave as observed with ozonesonde and rawinsondes, *J. Geophys. Res.*, *103*(D15), 19,173–19,182, 1998.

Fujiwara, M., F. Hasebe, M. Shiotani, N. Nishi, H. Vömel, and S. J. Oltmans, Water vapor control at the tropopause by equatorial Kelvin waves observed over the Galápagos, *Geophys. Res. Lett.*, *28*, 3143–3146, 2001.

Gettelman, A., J. R. Holton, and A. R. Douglass, Simulations of water vapor in the lower stratosphere and upper troposphere, *J. Geophys. Res.*, *105*(D7), 9003–9023, 2000.

Gettelman, A., W. J. Randel, F. Wu, and S. T. Massie, Transport of water vapor in the tropical tropopause layer, *Geophys. Res. Lett.*, *29*(1), 1009, doi:10.1029/2001GL013818, 2002.

Gill, A. E., Some simple solutions for heat-induced tropical circulation, *Q. J. R. Meteorol. Soc.*, *106*, 447–462, 1980.

Hatsushika, H., Observational and modeling studies on the three dimensional structure of the tropical tropopause and its interannual variation, Ph.D. thesis, Grad. School of Environ. Earth Sci., Hokkaido Univ., Sapporo, Japan, 2001.

Hatsushika, H., and K. Yamazaki, Interannual variations of temperature and vertical motion at the tropical tropopause associated with ENSO, *Geophys. Res. Lett.*, *28*, 2891–2894, 2001.

Highwood, E. J., and B. J. Hoskins, The tropical tropopause, *Q. J. R. Meteorol. Soc.*, *124*, 1579–1604, 1998.

Holton, J. R., and A. Gettelman, Horizontal transport and the dehydration of the stratosphere, *Geophys. Res. Lett.*, *28*, 2799–2802, 2001.

Jackson, D. R., J. Methven, and V. D. Pope, Transport in the low-latitude tropopause zone diagnosed using particle trajectories, *J. Atmos. Sci.*, *58*, 173–192, 2001.

Jensen, E. J., W. G. Read, J. Mergenthaler, B. J. Sandor, L. Pfister, and A. Tabazadeh, High humidities and subvisible cirrus near the tropical tropopause, *Geophys. Res. Lett.*, *26*, 2347–2350, 1999.

Le Treut, H., and Z.-X. Li, Sensitivity of an atmospheric general circulation model to prescribed SST changes: Feedback effects associated with the simulation of cloud optical properties, *Clim. Dyn.*, *5*, 175–187, 1991.

Matsuno, T., Quasi-geostrophic motions in the equatorial area, *J. Meteorol. Soc. Jpn.*, *44*, 25–43, 1966.

Moorthi, S., and M. J. Suarez, Relaxed Arakawa-Schubert: A parameterization of moist convection for general circulation models, *Mon. Weather Rev.*, *120*, 978–1002, 1992.

Nakajima, T., M. Tsukamoto, Y. Tsushima, and A. Numaguti, Modeling of the radiative process in a AGCM, in *Reports of a New Program for Creative Basic Research Studies, Studies of Global Environmental Change With Special Reference to Asia and Pacific Regions, Rep. I-3*, pp. 104–123, Cent. for Clim. Syst. Res., Tokyo, 1995.

Newell, R., and S. Gould-Stewart, A stratospheric fountain?, *J. Atmos. Sci.*, *38*, 2789–2796, 1981.

Norton, W. A., Longwave heating of the tropical lower stratosphere, *Geophys. Res. Lett.*, *28*, 3653–3656, 2001.

Numaguti, A., M. Takahashi, T. Nakajima, and A. Sumi, Development of an atmospheric general circulation model, in *Reports of a New Program for Creative Basic Research Studies, Studies of Global Environment Change With Special Reference to Asia and Pacific Regions, Rep. I-3*, pp. 1–27, Cent. for Clim. Syst. Res., Tokyo, 1995.

Randel, W. J., F. Wu, A. Gettelman, J. M. Russel III, J. M. Zawodny, and S. J. Oltmans, Seasonal variation of water vapor in the lower stratosphere observed in Halogen Occultation Experiment data, *J. Geophys. Res.*, *106*, 14,313–14,325, 2001.

Sherwood, S. C., A stratospheric "Drain" over the maritime continent, *Geophys. Res. Lett.*, *27*, 677–680, 2000.

Sherwood, S. C., and A. E. Dessler, On the control of stratospheric humidity, *Geophys. Res. Lett.*, *27*, 2513–2516, 2000.

Sherwood, S. C., and A. E. Dessler, A model for transport across the tropical tropopause, *J. Atmos. Sci.*, *58*, 765–779, 2001.

Simmons, A. J., A. Untch, C. Jacob, P. Kallberg, and P. Unden, Stratospheric water vapour and tropical tropopause temperatures in ECMWF analyses and multi-year simulations, *Q. J. R. Meteorol. Soc.*, *125*, 353–386, 1999.

H. Hatsushika, Central Research Institute of Electric Power Industry, Abiko Research Laboratory, 1646 Abiko, Abiko-shi, Chiba-ken 270-1194, Japan. (hatusika@criepi.denken.or.jp)

K. Yamazaki, Graduate School of Environmental Earth Science, Hokkaido University, N10W5, Sapporo, Hokkaido, 060-0810, Japan. (yamazaki@ees.hokudai.ac.jp)